Batteries & Supercaps

Research Article
doi.org/10.1002/batt.202200009

Chemistry Europe
European Chemical Societies Publishing

www.batteries-supercaps.org

Special Collection

Highly Stable, Low Redox Potential Quinone for Aqueous Flow Batteries**

Min Wu,[a] Meisam Bahari,[a] Yan Jing,[b] Kiana Amini,[a] Eric M. Fell,[a] Thomas Y. George,[a] Roy G. Gordon,*[b] and Michael J. Aziz*[a]

Aqueous organic redox flow batteries are promising candidates for large-scale energy storage. However, the design of stable and inexpensive electrolytes is challenging. Here, we report a highly stable, low redox potential, and potentially inexpensive negolyte species, sodium 3,3′,3″,3‴-((9,10-anthraquinone-2,6-diyl)bis(azanetriyl))tetrakis(propane-1-sulfonate) (2,6-N-TSAQ), which is synthesized in a single step from inexpensive precursors. Pairing 2,6-N-TSAQ with potassium ferrocyanide at pH = 14 yielded a battery with the highest open-circuit voltage, 1.14 V, of any anthraquinone-based cell with a capacity fade rate < 10%/yr. When 2,6-N-TSAQ was cycled at neutral pH, it exhibited two orders of magnitude higher capacity fade rate. The great difference in anthraquinone cycling stability at different pH is interpreted in terms of the thermodynamics of the anthrone formation reaction. This work shows the great potential of organic synthetic chemistry for the development of viable flow battery electrolytes and demonstrates the remarkable performance improvements achievable with an understanding of decomposition mechanisms.

Introduction

Safe and economical energy storage technologies are indispensable for the deep penetration of intermittent renewable energies such as photovoltaic and wind electricity.[1] Aqueous redox flow batteries are promising candidates for large-scale energy storage compared to other storage devices such as pumped-hydro, flywheel, and lithium-ion batteries, owing to the highly modular configuration, long cycle life, and good safety features.[1b,c] Aqueous vanadium redox flow batteries (VRFBs) have been successfully established by many manufacturers, due to their long cycling life and high-power density.[2] However, cost reductions in VRFBs are anticipated to be difficult due to the abundance of vanadium and its fluctuating price. Consequently, aqueous organic redox flow batteries (AORFBs) are attracting tremendous research interest, as the redox active materials comprising earth abundant elements are potentially inexpensive.[1c,3] Additionally, the physical and electrochemical properties of redox organics, such as aqueous solubility, molecular size, molecular net charge, redox potential, and chemical stability could be tailored for improved performance via molecular functionalization.[4]

One drawback of many reported AORFBs, however, is their fast capacity fade because redox organics are susceptible to degradation reactions such as nucleophilic substitution, disproportionation, and tautomerization.[1c] To date, various redox-active organics based on quinone,[4,5] viologen,[6] phenazine,[7] alloxazine,[8] ferrocene[6b,c,9] and nitroxide radical derivatives[6a,g,7a,10] have been reported for AORFBs. Most of them, however, exhibit high-capacity fade rates of 0.1%–1%/day,[1c] which is unsuitable for practical application. Recently, anthraquinone derivatives such as 2,6-DBEAQ, 2,6-DPPEAQ, DPivOHAQ and DBAQ have demonstrated very good long-term stability.[5b,g,j] However, their widespread application is hindered by the high synthetic cost due to sophisticated synthesis or expensive precursors involved. Additionally, there is an apparent trade-off between anthraquinone cycling stability and the redox potential.[11] The highly stable anthraquinones such as 2,6-DBEAQ, DPivOHAQ, and DBAQ have a redox potential more positive than −0.52 V vs. standard hydrogen electrode (SHE) at pH = 12 and above; anthraquinones with a more negative redox potential exhibited less stable cycling performance.[4a,12] For a negolyte molecule, however, a low redox potential is desired to achieve high cell voltage. Therefore, developing inexpensive and stable anthraquinone negolytes with a low redox potential remains crucial for the practical implementation of AORFBs.

Here, we report a potentially inexpensive and low redox-potential anthraquinone negolyte with outstanding cycling stability. The anthraquinone sodium 3,3′,3″,3‴-((9,10-anthraquinone-2,6-diyl)bis(azanetriyl))tetrakis(propane-1-sulfonate) (2,6-N-TSAQ) was synthesized from inexpensive 2,6-diaminoanthraquinone (2,6-DAAQ) via a one-step N-alkylation route. The

[a] Dr. M. Wu, Dr. M. Bahari, Dr. K. Amini, E. M. Fell, T. Y. George, Prof. M. J. Aziz
John A. Paulson School of Engineering and Applied Sciences
Harvard University, Cambridge
02138 Massachusetts, United States
E-mail: maziz@harvard.edu
[b] Dr. Y. Jing, Prof. R. G. Gordon
Department of Chemistry and Chemical Biology
Harvard University, Cambridge
02138 Massachusetts, United States
E-mail: gordon@chemistry.harvard.edu

[**] A previous version of this manuscript has been deposited on a preprint server (https://doi.org/10.26434/chemrxiv-2021-rjzdn).

Supporting information for this article is available on the WWW under https://doi.org/10.1002/batt.202200009

Special Collection An invited contribution to a Special Collection dedicated to Organic Batteries

Research Article
doi.org/10.1002/batt.202200009

redox potential of 2,6-N-TSAQ at pH = 12 and above is −0.62 V vs. SHE, which is 120 mV lower than that of the oxygen-linked anthraquinone sodium 3,3′-((9,10-anthraquinone-2,6-diyl)bis(oxy))bis(propane-1-sulfonate) (2,6-O-DPSAQ) and 170 mV lower than that of the carbon-linked anthraquinone sodium 3,3′-(9,10-anthraquinone-2,6-diyl)bis(propane-1-sulfonate) (2,6-DPSAQ). Pairing with ferro/ferricyanide, it yields a cell with an open circuit potential of 1.14 V and a peak power density of 0.18 W/cm^2 at pH = 14. The capacity fade rate of 2,6-N-TSAQ is 0.025 %/day at pH = 14, yielding the highest open-circuit voltage of any anthraquinone-based cell with a capacity fade < 10 %/yr. Greater capacity fade rates by up to two orders of magnitude at near-neutral pH are interpreted in terms of changes in the driving free energy for anthrone formation. These results provide guidance for improving the performance of anthraquinone negolytes and highlight the great potential of organic synthesis towards inexpensive and stable electrolytes for grid-scale energy storage application.

Results and Discussion

Figure 1 illustrates the synthetic routes for three different anthraquinones 2,6-N-TSAQ, 2,6-O-DPSAQ and 2,6-DPSAQ. The structure of 2,6-N-TSAQ was verified by ^{1}H nuclear magnetic resonance (NMR) and high-resolution liquid chromatography-mass spectrometry as shown in Figures S1 and S2. The structures of 2,6-O-DPSAQ and 2,6-DPSAQ were verified by ^{1}H NMR as shown in Figures S3 and S4. Among them, 2,6-N-TSAQ and 2,6-O-DPSAQ were synthesized via similar one-step nucleophilic substitution reactions. 2,6-N-TSAQ was produced from 2,6-DAAQ, and 2,6-O-DPSAQ was synthesized from 2,6-dihydroxyanthraquinone (2,6-DHAQ). In both cases, sodium hydride was used to fully deprotonate the anthraquinone precursors in anhydrous dimethyl sulfoxide or N,N-dimethylformamide. Afterward, the deprotonated anthraquinone precursors react with 1,3-propanesultone overnight at room temperature to afford 2,6-N-TSAQ or 2,6-O-DPSAQ. Benefiting from the high reactivity of 1,3-propanesultone, the reaction is readily performed at room temperature with high purity and yield, making it very suitable for mass production. In contrast, 2,6-DPSAQ was synthesized from 2,6-DAAQ with three steps.[13] First, 2,6-DAAQ was converted to 2,6-diiodoanthraquinone. Afterward, it reacted with sodium allylsulfonate via Heck reaction followed by a hydrogenation step to yield 2,6-DPSAQ. The three-step reaction involving precious metal catalysts makes it less attractive compared with the one-step synthesis of 2,6-N-TSAQ and 2,6-O-DPSAQ. Since the laboratory cost of precursor 2,6-DAAQ is much lower than that of 2,6-DHAQ (Table S1), 2,6-N-TSAQ could be the most inexpensive anthraquinone among the three at a mass production scale, decreasing the capital cost of AORFBs.

Figure 2(a) exhibits the cyclic voltammograms (CV) of 2,6-DPSAQ, 2,6-O-DPSAQ, and 2,6-N-TSAQ. The redox potential of 2,6-N-TSAQ is −0.62 V vs. SHE in 1 M NaCl, which is 120 mV and 170 mV lower than that of 2,6-O-DPSAQ and 2,6-DPSAQ in 1 M

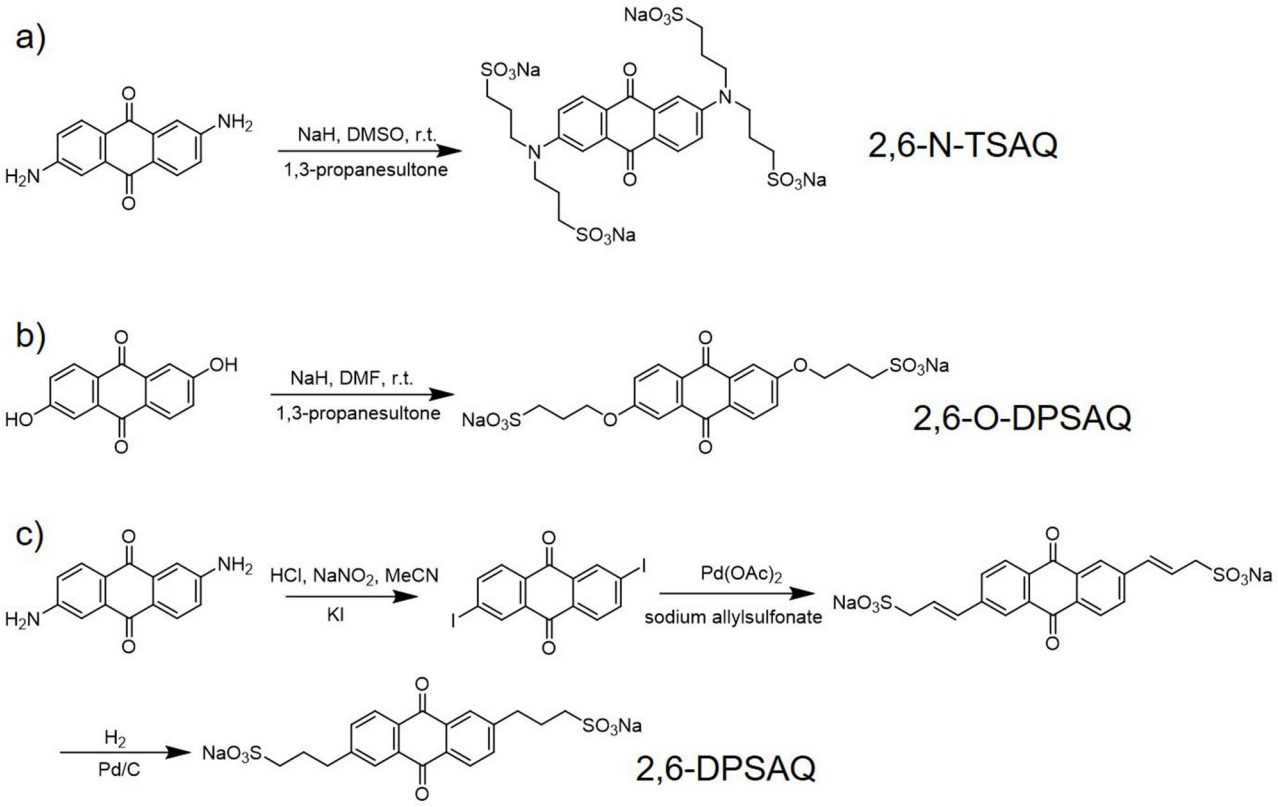

Figure 1. Synthetic routes for three different anthraquinones. a) 2,6-N-TSAQ; b) 2,6-O-DPSAQ; c) 2,6-DPSAQ.

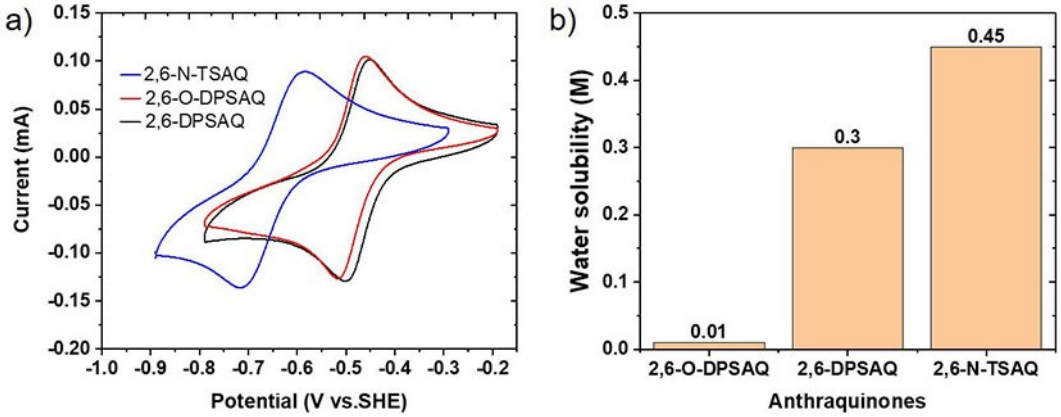

Figure 2. a) Cyclic voltammograms of 5 mM 2,6-N-TSAQ and 5 mM 2,6-DPSAQ in 1 M sodium chloride, and 5 mM 2,6-O-TSAQ in 1 M lithium chloride, each with a scan rate of 100 mV/s; b) solubility comparison for 2,6-N-TSAQ, 2,6-O-DPSAQ and 2,6-DPSAQ in deionized water.

NaCl, respectively. The low redox potential of 2,6-N-TSAQ is attributed to the strong electron donating effect of nitrogen lone pairs. It contributes to form a high working voltage and high-power density flow battery. The CV of 2,6-N-TSAQ in 1 M NaOH is shown in Figure S5. The redox potential of 2,6-N-TSAQ at pH = 14 is −0.63 V vs. SHE, which is close to that in 1 M sodium chloride medium. But the peak separation of 2,6-N-TSAQ in 1 M NaOH (94 mV) is much smaller than that in 1 M NaCl (130 mV), indicating a much faster redox process at pH = 14 than that at lower pH. The water solubility of 2,6-DPSAQ, 2,6-O-DPSAQ, and 2,6-N-TSAQ is shown in Figure 2(b). Surprisingly, 2,6-O-DPSAQ exhibited an extremely low solubility of 10 mM in deionized water and in 1 M lithium chloride, and an even lower solubility of less than 5 mM in 1 M sodium chloride and 1 M potassium chloride. The general water solubility trend for such sulfonate molecules is Li^+ form > Na^+ form > K^+ form; this differs from those for carboxylate and phenolate molecules, which normally exhibit the highest solubility in K^+ form. The solubilities of 2,6-DPSAQ and 2,6-N-TSAQ in deionized-water (no supporting salt) are 0.3 M and 0.45 M, respectively. In 1 M NaOH medium, the solubility of 2,6-N-TSAQ decreases to 0.4 M.

Given the higher water solubility, lower redox potential, and possible lower synthetic cost, 2,6-N-TSAQ was selected for further electrochemical study. The advantage of 2,6-N-TSAQ over some other low redox potential anthraquinones[4a,12] is that it has four negative charges on the solubilizing groups, leading to a high intermolecular Coulomb repulsion and a low collision rate. According to Marcus theory,[14] these properties could decrease the reaction rate of the disproportionation (known to cause capacity decay in anthraquinone negolyte).[5j,11] The large Coulomb repulsion and bulky functionalization also decrease the molecular permeability across cation exchange membranes, increasing the cell lifetime. The permeability of 2,6-N-TSAQ through sodium-exchanged Nafion NR212 was measured in a two-compartment diffusion cell. Due to a very low crossover rate, we estimate a maximum permeability of 3×10^{-14} cm^2/s (Figure S7), which is even lower than that reported for the tetra-anionic anthraquinone derivative 2,6-DPPEAQ.[5g]

The Pourbaix diagram of 2,6-N-TSAQ, shown in Figure 3a, indicates the molecule undergoes a two-proton/two-electron process below pH = 10, a one-proton/two-electron process over pH = 10–12, and a pH-independent two-electron process at pH > 12 with a redox potential around −0.63 V vs. SHE. The corresponding CV profiles at various pH are shown in Figure S8. It should be noted that the pH is the local pH of anthraquinone molecules. For an unbuffered case, e.g., 1 M NaCl, the formal potential of 2,6-N-TSAQ is −0.62 V, which is close to the redox potential at high pH; such a phenomenon was also observed in other anthraquinones when a pH buffer was not used.[5g,h] Based on the Pourbaix diagram, the pK_a1 and pK_a2 of reduced and protonated 2,6-N-TSAQ are estimated to have values around 10 and 12, respectively, which are slightly larger than those of anthraquinone negolytes with more positive redox potentials.[4b,5b,g,j] We attribute this to the strong electron donating effect of lone pair electrons on nitrogen atoms decreasing the pK_a of hydroxy groups of the 9,10-dihydroxyanthracene (reduced state of anthraquinone).

The electrochemical properties of 2,6-N-TSAQ were determined by rotating disk electrode (RDE) test as shown in Figures 3(b) and S9. The diffusion coefficient (D) was calculated to be 5.8×10^{-7} cm^2/s by the Levich equation. The charge transfer coefficient was determined to be 0.32 based on the Tafel equation, and the electron transfer rate constant was determined to be 2.53×10^{-4} cm/s.

Polarization experiments of a 0.1 M 2,6-N-TSAQ/ferrocyanide full cell at pH = 14 were performed at various states of charge. The electrolytes comprised 5 mL of 0.1 M 2,6-N-TSAQ (negolyte) at pH = 14 and 30 mL of 0.1 M potassium ferrocyanide and 0.02 M potassium ferricyanide (posolyte) at pH = 14 to ensure that the negolyte was always the capacity limiting side. The cell was constructed from graphite flow plates and AvCarb carbon cloth electrodes, separated by a Nafion 212 membrane ion exchanged in 1 M NaOH for over 12 hours at room temperature. The electrolyte was charged/discharged at 40 mA/cm^2 between 0.6 V and 1.4 V with a potential hold until the current dropped to 2 mA/cm^2 to get the full capacity. The OCV increased from 0.8 to 1.31 V as the SOC increased from

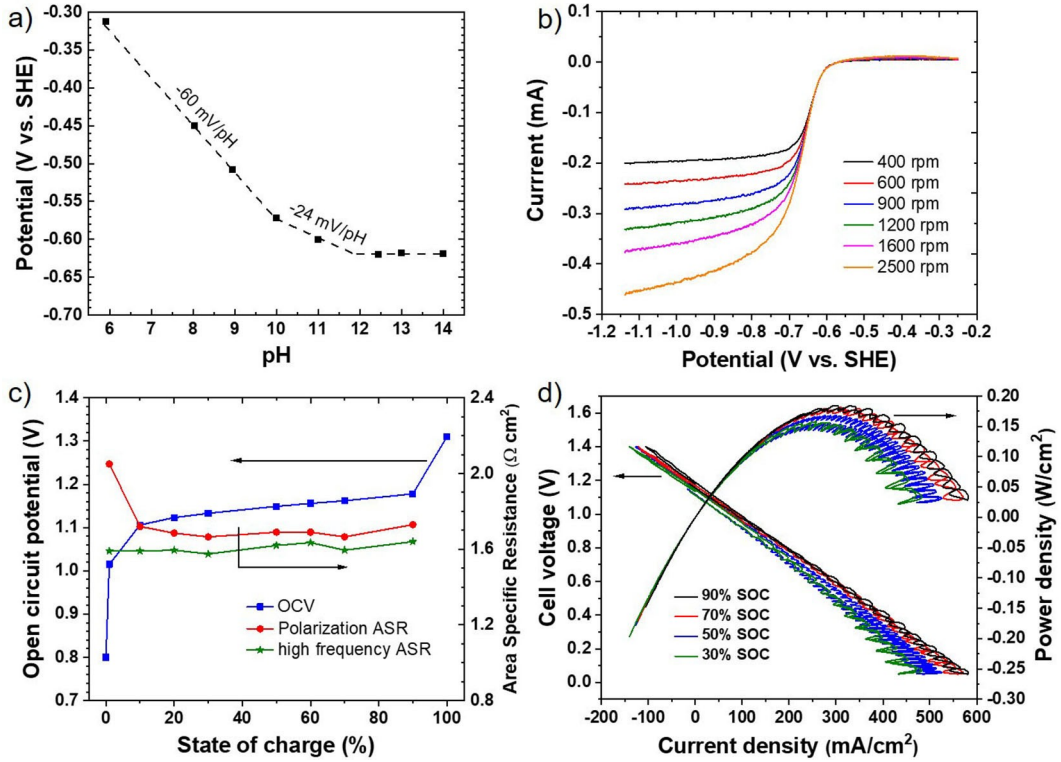

Figure 3. Electrochemical performance of 2,6-N-TSAQ. a) Pourbaix diagram of 2,6-N-TSAQ redox process; b) linear sweep voltammograms of 5 mM 2,6-N-TSAQ in 1 M NaOH on a glassy carbon rotating disk electrode at rotation rates between 400 and 2500 rpm; c) open circuit voltage (OCV), high-frequency area-specific resistance (ASR) and polarization ASR versus SOC of 2,6-N-TSAQ/potassium ferrocyanide full cell at pH = 14; d) polarization measurements of 2,6-N-TSAQ/potassium ferrocyanide full cell at pH = 14. Cell configuration in (c and d): 5 mL of 0.1 M 2,6-N-TSAQ pH = 14 | 30 mL of 0.1 M $K_4Fe(CN)_6$, 0.02 M $K_3Fe(CN)_6$, pH = 14 (1 M NaOH). Sodium exchanged Nafion® 212 was used as the ion-selective membrane between the AvCarb carbon cloth electrodes.

~0% to ~100% (Figure 3a). The 0.2 V increase of OCV from 0 to ~1% SOC, 0.09 V increase from ~1% to ~10%, 0.08 V increase from 10% to 90% SOC, and 0.14 V from 90% to final OCV, indicates the utilization of 2,6-N-TSAQ is more than 99% under the operating conditions according to the Nernst equation. The peak galvanic power density at 10% SOC was 0.15 W/cm^2 and increased to 0.18 W/cm^2 at 90% SOC (Figure 3d). The power density is mainly limited by the high-frequency ASR, which is dominated by the membrane resistance (Figure 3c) with a value around 1.6 Ω cm^2. Therefore, the power density is expected to be improved with a lower-resistance membrane.

A long-term cycling test of the 0.1 M 2,6-N-TSAQ/ferrocyanide flow battery at pH = 14 was performed with the same cell. The cell was cycled at 40 mA cm^{-2} with potential holds at 1.4 V for charging and 0.6 V for discharging until the current density dropped to 2 mA/cm^2. The initial volumetric discharge capacity was 4.76 Ah/L, corresponding to a capacity utilization of 88.9% of the theoretical value. However, the OCV at different SOCs in Figure 3(c) and the typical voltage profile in Figure 4(c) indicates it achieves full capacity of 2,6-N-TSAQ under such conditions. The difference between realized capacity and the theoretical value could come from errors in electrolyte volume measurement or the presence of non-redox active impurities such as water or salts in the sample or the relatively slow kinetics of 2,6-N-TSAQ. After 9 days of full SOC range cycling, the discharge capacity decreased to 4.75 Ah/L, corresponding to a temporal capacity fade rate of 0.025%/day or 0.00024%/cycle. The average coulombic efficiency was determined to be above 99.9%. The voltage/capacity profile at different cycles in Figure 4(c) are almost invariant, indicating the highly-stable cell performance of 2,6-N-TSAQ at pH = 14. This high cycling stability is achieved in an anthraquinone molecule with an unusually low redox potential.

An otherwise-identical 0.1 M 2,6-N-TSAQ/ferrocyanide full cell was cycled in 1 M NH_4Cl enabling the pH to remain below 10 over the entire SOC range. The initial charge capacity was up to 4.98 Ah/L but the initial discharge capacity was only 0.50 Ah/L with a low coulombic efficiency of 10.1% as shown in Figure S11. The discharge capacity dropped to 0.29 Ah/L in the third cycle with a coulombic efficiency around 80%. The ^{1}H NMR spectrum for the cycled 2,6-N-TSAQ (NH_4^+) is shown in Figure S12. The five peaks with asterisks in the aromatic region are similar to the anthrone peaks observed in 2,6-DHAQ,[11] suggesting that the major decomposition of 2,6-N-TSAQ came from anthrone formation. After the electrolyte was fully oxidized by exposure to air, the five peaks with asterisks disappeared and some new peaks appeared, suggesting that the anthrone was oxidized to anthraquinone and anthrone dimer.[5j,11] Furthermore, mass spectrometry was used to analyze the cycled 2,6-N-TSAQ (NH_4^+) electrolyte, and anthrone was detected as the major decomposition compound (Figure S13).

Research Article
doi.org/10.1002/batt.202200009
Chemistry Europe
European Chemical Societies Publishing

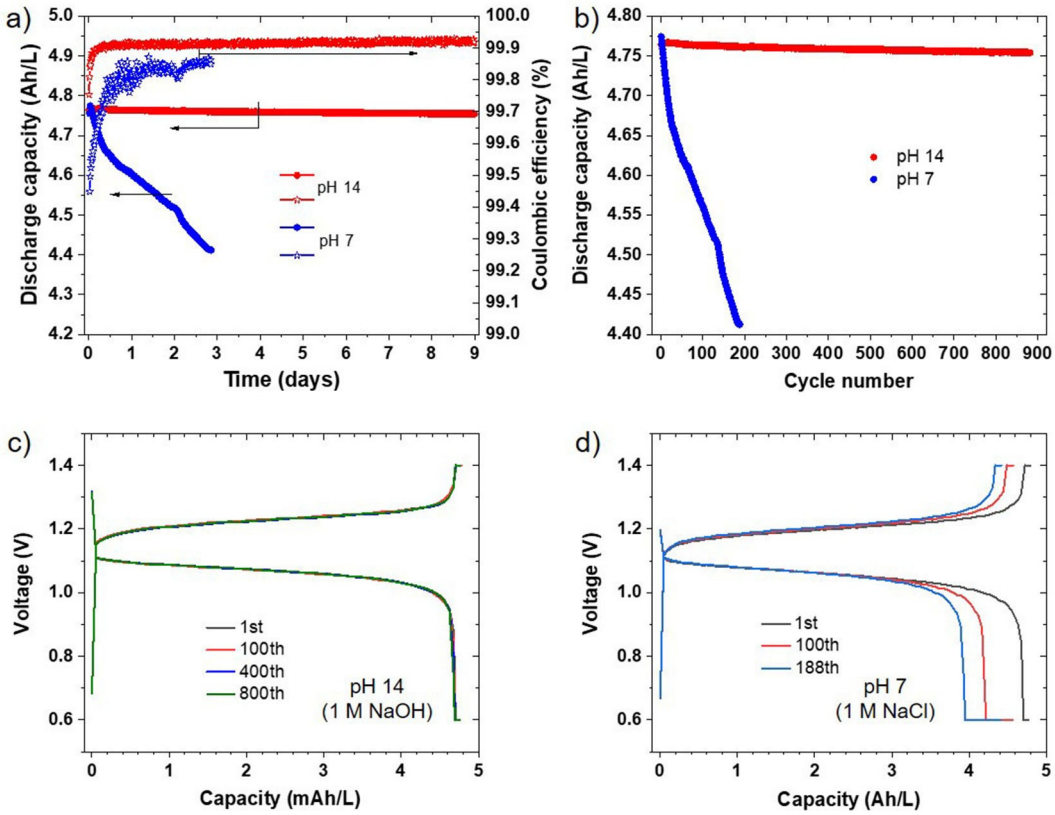

Figure 4. Cell performance of 0.1 M 2,6-N-TSAQ/ferrocyanide cell, 2,6-N-TSAQ as the capacity limiting side. a) Discharge capacity and Coulombic efficiency versus cycle time at pH = 7 and 14; b) discharge capacity versus cycle number at pH = 7 and 14; c) charge-discharge voltage profile of 2,6-N-TSAQ from selected cycles at pH = 14 in (b); d) charge-discharge voltage profile of 2,6-N-TSAQ from selected cycles at pH = 7 in (b). Untreated AvCarb carbon cloth was used as the electrodes, and sodium or ammonium exchanged Nafion® 212 was the ion-selective membrane.

To investigate the origin of cycling instability of 2,6-N-TSAQ under neutral conditions, both oxidized and reduced forms of 2,6-N-TSAQ were stored in 1 M NaCl at 45 °C for 8 days. No apparent decomposition was found in the ^{1}H NMR of the oxidized state in Figure S14. In contrast, the reduced 2,6-N-TSAQ sample showed a large quantity of decomposition after 1 week, implying that the reduced form of 2,6-N-TSAQ undergoes the disproportionation reaction, which is well-known in anthraquinone negolytes, at pH = 7. In contrast, only a minor amount of decomposition was detected for the reduced sample when the reduced 2,6-N-TSAQ was stored in 1 M NaOH at 45 °C for 8 days.

We interpret the substantial difference in the stability of reduced anthraquinone at pH = 7 and 14 in terms of the thermodynamics of anthrone formation. The disproportionation reaction of 9,10-dihydroxyanthracene is the sum of half reactions I and II in Figure 5(a). The Gibbs free energy change $\Delta G^{\circ\prime}$ of the disproportionation reaction under standard conditions except that the pH is fixed at a certain value can be expressed as, where E_1 and E_2 are the redox potentials of the two half-reactions under these conditions. The proposed Pourbaix diagram of anthraquinone, 9,10-dihydroxyanthracene, and anthrone is shown in Figure 5(b). The state of protonation of the molecules on the left-hand side of Reactions I and II is illustrated in the intermediate-potential band of the Pourbaix diagram. When the local pH < pK_a1, both half reactions undergo a two-proton/two-electron process. When the local pH is between p*K*a1 and p*K*a, reaction I undergoes a one-proton/two-electron process, and reaction II undergoes a three-proton/two-electron reaction. When pK_a < pH < pK_a2, reaction I still experiences one-proton/two-electron process, while reaction II undergoes a two-proton/two-electron process. When pH is above pK_a2, half reaction I becomes pH independent, and half reaction II undergoes a three-proton/two-electron reaction. As shown in Figure 5(b), the Gibbs free energy change for anthrone formation is around $\Delta\left(\Delta G^{\circ\prime}\right) = -2 \times \frac{96485C}{mol} \times \frac{-\frac{0.089\ V}{pH} \times 2pH}{1000} = 34$ kJ/mol less negative at pH = 14 than that at pH = 12. Similarly, the difference in Gibbs free energy change per mole of anthrone formation at pH = 14 and 10 could be as large as $-2 \times 96485 \times (0.089 \times 3 + 0.0295 \times 1)/1000 = 57$ kJ/mol, if pK_a is around 10 and pK_a2 is around 11. Therefore, anthrone formation becomes significantly more disfavored at pH = 14 than that at a significantly lower pH. Consequently, when anthrone formation is the predominant decomposition mechanism, anthraquinone-based flow batteries exhibit better cycling performance at high pH than that at lower pH. Moreover, the Gibbs free energy change for the anthrone formation reaction at a 100% SOC (no anthrone and anthraquinone, 100% 9,10-dihydroxyanthracene) is always

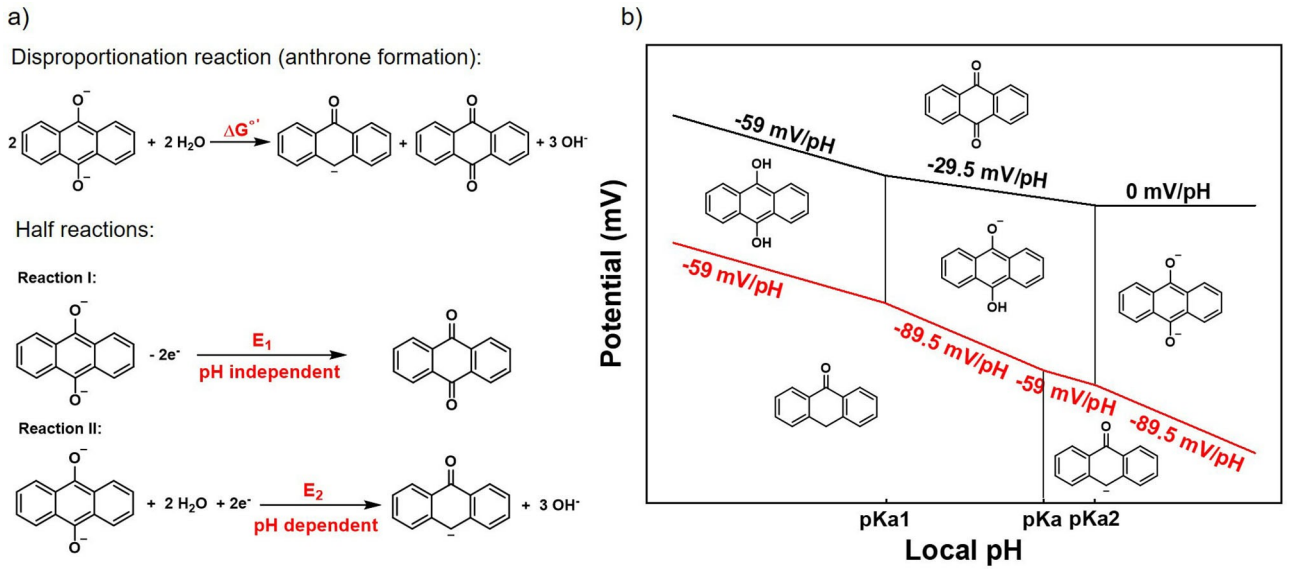

Figure 5. a) Disproportionation reaction of 9,10-dihydroxyanthraceen at pH above its pK_a2 and the corresponding two half reactions; b) representative Pourbaix diagram of anthraquinone, 9,10-dihydroxyanthracene, and anthrone. The pK_a1 and pK_a2 belong to 9,10-dihydroxyanthracene, and pK_a (around 10) belongs to anthrone.[16] The water molecules in the half reactions were neglected in (b) due to the space limitation.

negative, indicating that for any given anthraquinone, the disproportionation reaction at the full SOC is always thermodynamically favorable. When the SOC of anthraquinone increases from 90% to 99%, the Gibbs free energy change for anthrone formation becomes more negative by approximately 8.414 J/mol/K$\times\left(\ln\frac{0.1}{0.9^2}-\ln\frac{0.01}{0.99^2}\right)$ assuming the variation of anthrone concentration is negligible. Likewise, when the SOC of anthraquinone negolyte increases from 90% to 99.9%, the Gibbs free energy change for anthrone formation becomes more negative by approximately 11.93 kJ/mol. Therefore, to suppress anthrone formation in practical deployment, charging to a high SOC should be avoided, i.e., it is desired not to conduct a potential hold at the end of the charging half-cycle. A simple galvanostatic cycling protocol, however, cannot be used in research to evaluate very low-capacity fade rates.[1c,15] For future research on anthraquinone negolytes species, a potential hold after, say, every 30 cycles of galvanostatic cycling might be advisable.

In summary, we synthesized three sulfonated anthraquinone derivatives, carbon-linked, nitrogen-linked, and oxygen-linked. The nitrogen-linked anthraquinone (2,6-N-TSAQ) showed a much lower redox potential than the others due to the strongest electron donating effect of lone pair electrons on nitrogen atoms. Because it is synthesized from inexpensive precursor with a one-step N-alkylation method, the mass production cost could be low. Despite the Coulomb repulsion afforded by its four negatively charged sulfonate groups, the cycling performance of 2,6-N-TSAQ is poor at neutral pH, with a capacity fade rate of 2.6%/day. The cycling stability improved by two orders of magnitude to 0.025%/day by raising the pH to 14. The 2,6-N-TSAQ|ferro/ferricyanide cell at pH = 14 exhibits the highest open-circuit voltage, 1.14 V, of any anthraquinone-based cell with a capacity fade rate no greater than <10%/yr. The great difference in anthraquinone cycling stability at different pH values is explained in terms of the thermodynamics of anthrone formation. This work demonstrates the significant improvement in performance that can be made with a better understanding of capacity fade mechanisms and illustrates the great potential of organic synthetic chemistry for low-cost and stable AORFB electrolytes.

Acknowledgements

This research was supported by the U.S. National Science Foundation through grant CBET-1914543 and by U.S. DOE award DE-AC05-76RL01830 through PNNL subcontract 535264. The authors thank Martin Jin, Emily Kerr, Daniel Pollack, and Jinxu Gao for valuable discussions. We dedicate this paper to the memory of Professor Susan A. Odom, who was an inspiring collaborator, teacher, and friend.

Conflict of Interest

M. B., R. G. G. and M. J. A. have ownership stakes in Quino Energy, Inc., which may profit from the results reported here.

Data Availability Statement

The data that support the findings of this study are available from the corresponding author upon reasonable request.

Keywords: anthraquinone · aqueous flow batteries · cost effective · low redox potential · stable

[1] a) B. Dunn, H. Kamath, J. M. Tarascon, *Science* **2011**, *334*, 928–935; b) G. L. Soloveichik, *Chem. Rev.* **2015**, *115*, 11533–11558; c) D. G. Kwabi, Y. Ji, M. J. Aziz, *Chem. Rev.* **2020**, *120*, 6467–6489.
[2] M. Ulaganathan, V. Aravindan, Q. Yan, S. Madhavi, M. Skyllas-Kazacos, T. M. Lim, *Adv. Mater. Interfaces* **2016**, *3*, 1500309.
[3] a) J. A. Luo, B. Hu, M. W. Hu, Y. Zhao, T. L. Liu, *ACS Energy Lett.* **2019**, *4*, 2220–2240; b) J. Winsberg, T. Hagemann, T. Janoschka, M. D. Hager, U. S. Schubert, *Angew. Chem. Int. Ed.* **2017**, *56*, 686–711; *Angew. Chem.* **2017**, *129*, 702–729; c) X. L. Wei, W. X. Pan, W. T. Duan, A. Hollas, Z. Yang, B. Li, Z. M. Nie, J. Liu, D. Reed, W. Wang, V. Sprenkle, *ACS Energy Lett.* **2017**, *2*, 2187–2204.
[4] a) K. Lin, Q. Chen, M. R. Gerhardt, L. Tong, S. B. Kim, L. Eisenach, A. W. Valle, D. Hardee, R. G. Gordon, M. J. Aziz, M. P. Marshak, *Science* **2015**, *349*, 1529–1532; b) B. T. Huskinson, M. P. Marshak, C. Suh, S. Er, M. R. Gerhardt, C. J. Galvin, X. Chen, A. Aspuru-Guzik, R. G. Gordon, M. J. Aziz, *Nature* **2014**, *505*, 195–198.
[5] a) M. R. Gerhardt, L. Tong, R. Gomez-Bombarelli, Q. Chen, M. P. Marshak, C. J. Galvin, A. Aspuru-Guzik, R. G. Gordon, M. J. Aziz, *Adv. Energy Mater.* **2017**, *7*, 1601488; b) D. G. Kwabi, K. Lin, Y. Ji, E. F. Kerr, M.-A. Goulet, D. De Porcellinis, D. P. Tabor, D. A. Pollack, A. Aspuru-Guzik, R. G. Gordon, M. J. Aziz, *Joule* **2018**, *2*, 1907–1908; c) J. Y. Cao, M. Tao, H. P. Chen, J. Xu, Z. D. Chen, *J. Power Sources* **2018**, *386*, 40–46; d) Z. Yang, L. Tong, D. P. Tabor, E. S. Beh, M. A. Goulet, D. De Porcellinis, A. Aspuru-Guzik, R. G. Gordon, M. J. Aziz, *Adv. Energy Mater.* **2018**, *8*, 1702056; e) C. X. Wang, Z. Yang, Y. R. Wang, P. Y. Zhao, W. Yan, G. Y. Zhu, L. B. Ma, B. Yu, L. Wang, G. G. Li, J. Liu, Z. Jin, *ACS Energy Lett.* **2018**, *3*, 2404–2409; f) L. Tong, M.-A. Goulet, D. P. Tabor, E. F. Kerr, D. De Porcellinis, E. M. Fell, A. Aspuru-Guzik, R. G. Gordon, M. J. Aziz, *ACS Energy Lett.* **2019**, *4*, 1880–1887; g) Y. Ji, M. A. Goulet, D. A. Pollack, D. G. Kwabi, S. Jin, D. Porcellinis, E. F. Kerr, R. G. Gordon, M. J. Aziz, *Adv. Energy Mater.* **2019**, *9*, 1900039; h) S. Jin, Y. Jing, D. G. Kwabi, Y. Ji, L. Tong, D. De Porcellinis, M. A. Goulet, D. A. Pollack, R. G. Gordon, M. J. Aziz, *ACS Energy Lett.* **2019**, *4*, 1342–1348; i) B. Hu, J. Luo, M. Hu, B. Yuan, T. L. Liu, *Angew. Chem. Int. Ed.* **2019**, *58*, 16629–16636; *Angew. Chem.* **2019**, *131*, 16782–16789; j) M. Wu, Y. Jing, A. A. Wong, E. M. Fell, S. Jin, Z. Tang, R. G. Gordon, M. J. Aziz, *Chem* **2020**, *6*, 1432–1442; k) Y. Jing, M. Wu, A. A. Wong, E. M. Fell, S. Jin, D. A. Pollack, E. F. Kerr, R. G. Gordon, M. J. Aziz, *Green Chem.* **2020**, *22*, 6084–6092; l) M. Wu, M. Bahari, E. Fell, R. G. Gordon, M. J. Aziz, *J. Mater. Chem. A* **2021**, *9*, 26709–26716.
[6] a) T. B. Liu, X. L. Wei, Z. M. Nie, V. Sprenkle, W. Wang, *Adv. Energy Mater.* **2015**, *6*, 1501449; b) B. Hu, C. DeBruler, Z. Rhodes, T. L. Liu, *J. Am. Chem. Soc.* **2017**, *139*, 1207–1214; c) E. S. Beh, D. De Porcellinis, R. L. Gracia, K. T. Xia, R. G. Gordon, M. J. Aziz, *ACS Energy Lett.* **2017**, *2*, 639–644; d) J. Luo, B. Hu, C. Debruler, T. L. Liu, *Angew. Chem. Int. Ed.* **2018**, *57*, 231–235; *Angew. Chem.* **2018**, *130*, 237–241; e) B. Hu, Y. Tang, J. Luo, G. Grove, Y. Guo, T. L. Liu, *Chem. Commun.* **2018**, *54*, 6871–6874; f) C. DeBruler, B. Hu, J. Moss, J. Luo, T. L. Liu, *ACS Energy Lett.* **2018**, *3*, 663–668; g) Y. H. Liu, M. A. Goulet, L. C. Tong, Y. Z. Liu, Y. L. Ji, L. Wu, R. G. Gordon, M. J. Aziz, Z. J. Yang, T. W. Xu, *Chem* **2019**, *5*, 1861–1870; h) W. Liu, Y. Liu, H. Zhang, C. Xie, L. Shi, Y. G. Zhou, X. Li, *Chem. Commun.* **2019**, *55*, 4801–4804; i) S. Jin, E. M. Fell, L. Vina-Lopez, Y. Jing, P. W. Michalak, R. G. Gordon, M. J. Aziz, *Adv. Energy Mater.* **2020**, *10*, 2000100; j) Y. Liu, Y. Li, P. Zuo, Q. Chen, G. Tang, P. Sun, Z. Yang, T. Xu, *ChemSusChem* **2020**, *13*,2245–2249.
[7] a) J. Winsberg, C. Stolze, S. Muench, F. Liedl, M. D. Hager, U. S. Schubert, *ACS Energy Lett.* **2016**, *1*, 976–980; b) A. Hollas, X. L. Wei, V. Murugesan, Z. M. Nie, B. Li, D. Reed, J. Liu, V. Sprenkle, W. Wang, *Nat. Energy* **2018**, *3*, 508–514; c) C. Wang, X. Li, B. Yu, Y. Wang, Z. Yang, H. Wang, H. Lin, J. Ma, G. Li, Z. Jin, *ACS Energy Lett.* **2020**, *5*, 411–417; d) S. Pang, X. Wang, P. Wang, Y. Ji, *Angew. Chem. Int. Ed.* **2021**, *60*, 5289–5298; *Angew. Chem.* **2021**, *133*, 5349–5358.
[8] K. Lin, R. Gomez-Bombarelli, E. S. Beh, L. Tong, Q. Chen, A. Valle, A. Aspuru-Guzik, M. J. Aziz, R. G. Gordon, *Nat. Energy* **2016**, *1*, 16102.
[9] a) Z. Zhao, B. Zhang, B. R. Schrage, C. J. Ziegler, A. Boika, *ACS Appl. Energ. Mater.* **2020**, *3*, 10270–10277; b) Y. Li, Z. Xu, Y. Liu, S. Jin, E. M. Fell, B. Wang, R. G. Gordon, M. J. Aziz, Z. Yang, T. Xu, *ChemSusChem* **2020**, *14*, 745–752.
[10] J. Winsberg, T. Janoschka, S. Morgenstern, T. Hagemann, S. Muench, G. Hauffman, J. F. Gohy, M. D. Hager, U. S. Schubert, *Adv. Mater.* **2016**, *28*, 2238–2243.
[11] M.-A. Goulet, L. Tong, D. A. Pollack, D. P. Tabor, S. A. Odom, A. Aspuru-Guzik, E. E. Kwan, R. G. Gordon, M. J. Aziz, *J. Am. Chem. Soc.* **2019**, *141*, 8014–8019.
[12] C. Wang, B. Yu, Y. Liu, H. Wang, Z. Zhang, C. Xie, X. Li, H. Zhang, Z. Jin, *Energy Storage Mater.* **2021**, *36*, 417–426.
[13] J. Yan, E. M. Fell, M. Wu, S. Jin, Y. Ji, D. A. Pollack, Z. Tang, D. Ding, M. Bahari, M.-A. Goulet, T. Tsukamoto, R. G. Gordon, M. J. Aziz, *ACS Energy Lett.* **2022**, *7*, 226–235.
[14] a) Y. K. Petit, E. Mourad, C. Prehal, C. Leypold, A. Windischbacher, D. Mijailovic, C. Slugovc, S. M. Borisov, E. Zojer, S. Brutti, O. Fontaine, S. A. Freunberger, *Nat. Chem.* **2021**, *13*, 465–471; b) R. A. Marcus, *Rev. Mod. Phys.* **1993**, *65*, 599–610.
[15] M.-A. Goulet, M. J. Aziz, *J. Electrochem. Soc.* **2018**, *165*, A1466-A1477.
[16] G. M. McCann, C. M. McDonnell, L. Magris, R. A.M. O'Ferrall, *J. Chem. Soc. Perkin Trans. 2* **2002**, 784–795.

Manuscript received: January 4, 2022
Accepted manuscript online: January 13, 2022
Version of record online: ■■, ■■■

RESEARCH ARTICLE

Organic negolyte electrolyte for flow batteries: Three anthraquinones with C, N, O- linked water-soluble chains have been synthesized and evaluated for aqueous flow batteries. The nitrogen linked anthraquinone showed the lowest redox potential of −0.62 V vs. SHE. Paired with ferrocyanide, it formed a cell voltage of 1.14 V with a capacity fade rate of 0.025%/day at pH = 14.

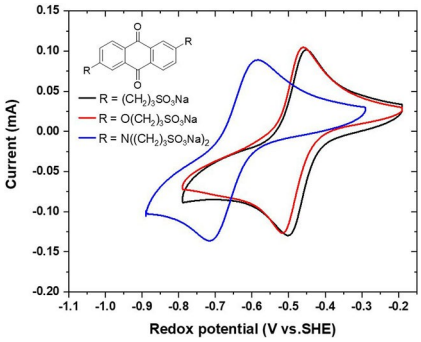

Dr. M. Wu, Dr. M. Bahari, Dr. Y. Jing, Dr. K. Amini, E. M. Fell, T. Y. George, Prof. R. G. Gordon, Prof. M. J. Aziz**

Batteries & Supercaps

Supporting Information

Highly Stable, Low Redox Potential Quinone for Aqueous Flow Batteries**

Min Wu, Meisam Bahari, Yan Jing, Kiana Amini, Eric M. Fell, Thomas Y. George, Roy G. Gordon,* and Michael J. Aziz*

Contents

Experimental Materials:

2,6-diaminoanthraquione (97%), 1,3-propanesultone (98%), sodium hydride (60% in mineral oil), anhydrous dimethyl sulfoxide, anhydrous N,N-Dimethylformamide, potassium carbonate, and palladium(II) acetate (98%) were purchased from Sigma-Aldrich. 2,6-dihydroxyanthraquinone (98%) was purchased from AK scientific. Sodium allylsulfonate (94%) was purchased from Ambeed, inc. Ltd. Hydrogen was purchased from Airgas. The materials were directly used without further purification.

Synthesis of 2,6-N-TSAQ

3 g of 2,6-diaminoanthraquinone (12.59 mmol) was added to 50 mL anhydrous dimethyl sulfoxide. Then 2.1 g sodium hydride (60%, 52.46 mmol) was added to the solution under vigorous stirring. After 15 minutes, 6.41 g 1,3-propanesultone (98%, 52.46 mmol) was added to the above mixture. The solution was stirred at room temperature for overnight. Afterward, ethyl acetate was added to the solution and collect the red solid. The crude product was further washed with ethyl acetate to remove any mineral oil. Yield:9.7 g (95%).

The ^{1}H NMR spectrum of 2,6-N-TSAQ is shown in Figure S1.

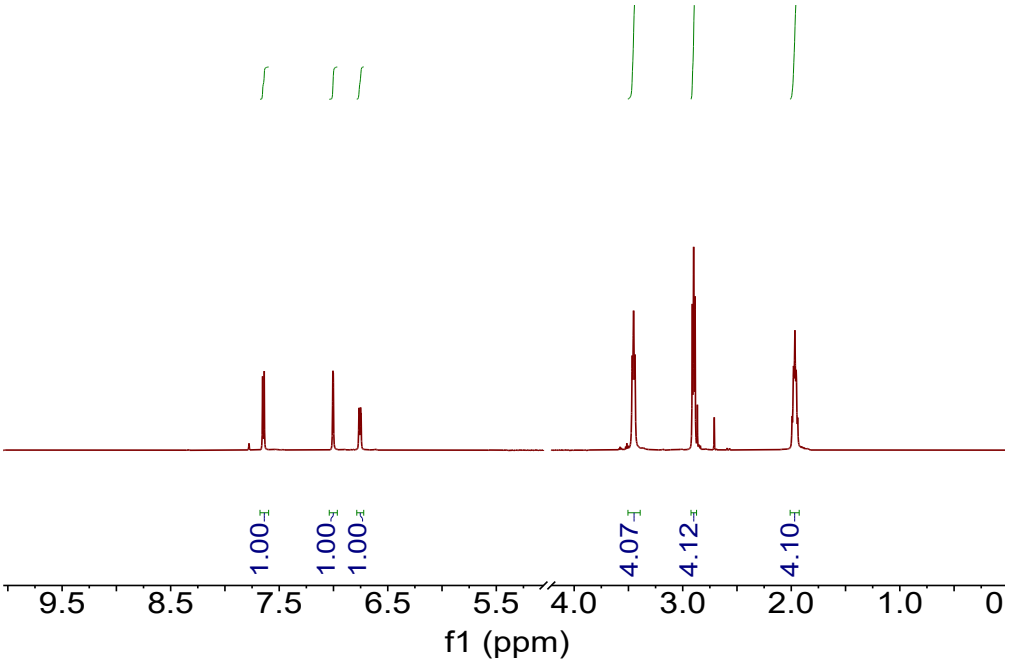

Figure S1. ^{1}H NMR spectrum of 2,6-N-TSAQ in D2O-d6. Solvent peak at 4.7 pm was censored to increase other peaks. ^{1}H NMR (500 MHz, D_2O) δ 7.65 (d, 2H), 7.00 (d, 2H), 6.76 (dd, 2H), 3.45 (t, 8H), 2.90 (t, 8H), 1.97 (m, 8H).

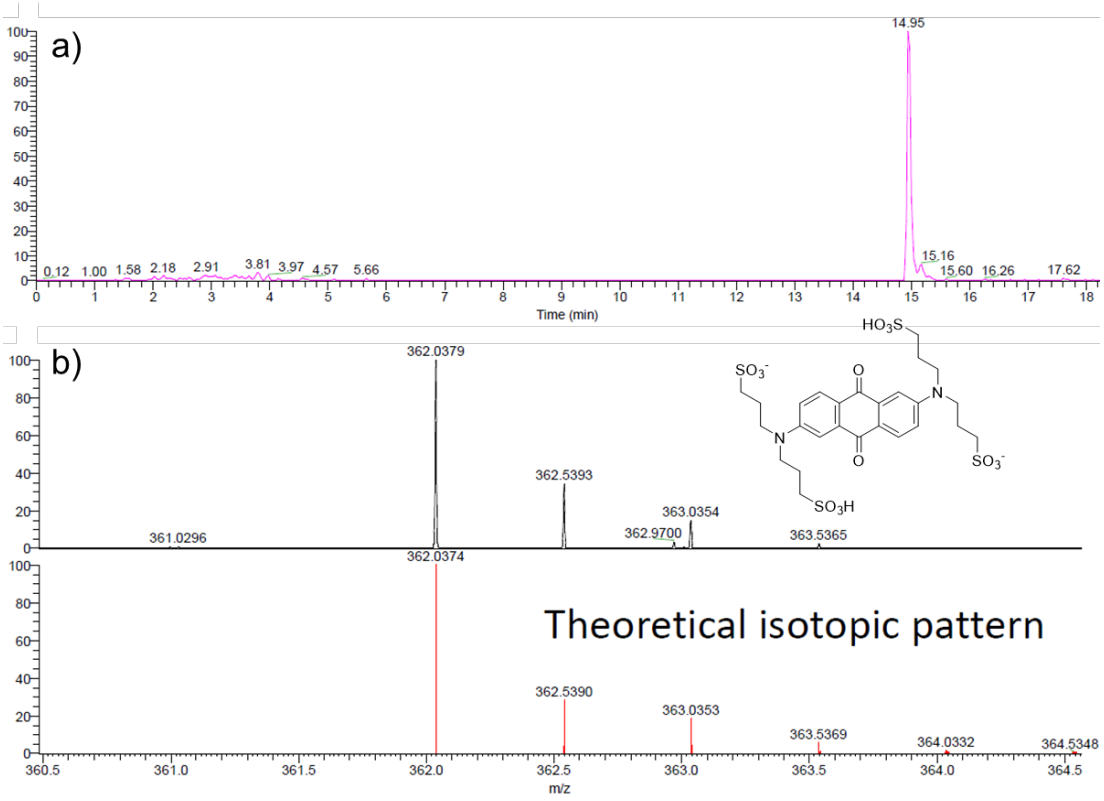

Figure S2. LC-MS traces of the synthesized 2,6-N-TSAQ. a) LC trace of 2,6-N-TSAQ; b) Mass spectrum of the material eluted at 14.95 min in the LC trace. The peak at m/z = 362.04 corresponding to the 2,6-N-TSAQ with two protonate form and two negative charges. Sample preparation: 0.1 M 2,6-N-TSAQ was diluted 100 times with HPLC water, and further diluted 100 times with acetonitrile/water co-solvents (V/V=1:1) to the desired concentration 10 μM. High-resolution LC-MS analysis was performed in the Small Molecule Mass Spectrometry Facility at Harvard University on a MiniLIMS. The elution solution is 0.1% v/v formic acid in acetonitrile. The ESI mass spectrum was recorded in negative ionization mode.

Synthesis of 2,6-O-DPSAQ

3 g of 2,6-dihydroxyanthraquinone (12.49 mmol) was added to 50 mL anhydrous N,N-Dimethylformamide. Then 1.05 g sodium hydride (60%, 26.23 mmol) was added to the solution under vigorous stirring. After 15 minutes, 3.20 g 1,3-propanesultone (98%, 26.23 mmol) was added to the above mixture. The solution was stirred at room temperature for overnight. Afterwards, ethyl acetate was added to the solution to collect the yellow solid. The crude product was washed with ethyl acetate to remove any mineral oil. Yield: 6.4 g (97%).

The ^{1}H NMR spectrum of 2,6-O-DPSAQ is shown in Figure S3.

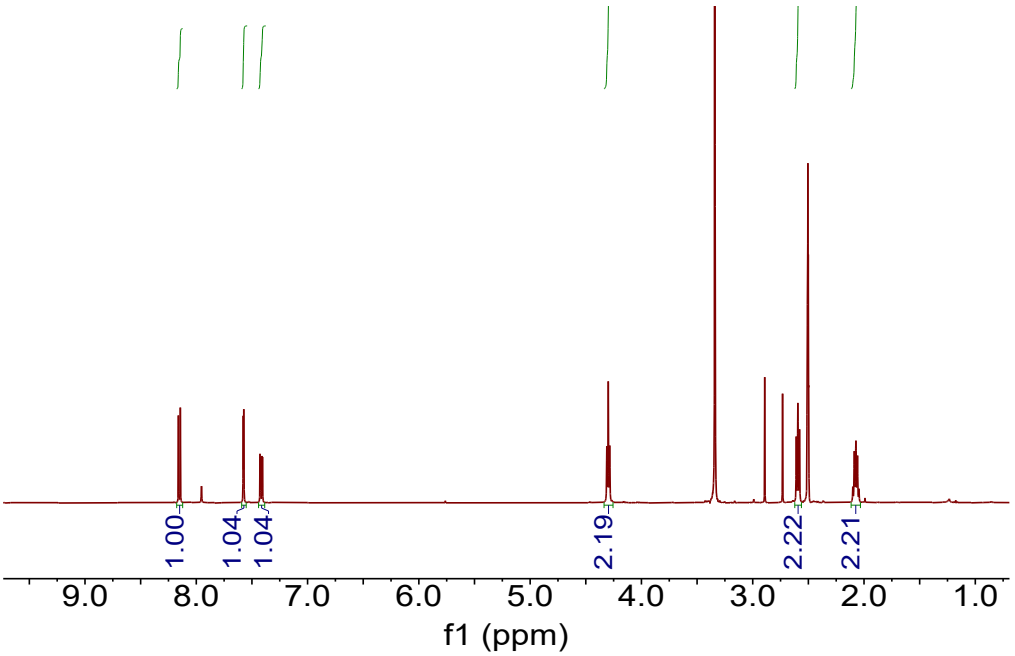

Figure S3. ^{1}H NMR spectrum of 2,6-O-DPSAQ in DMSO-d6. Solvent peaks are those not integrated. ^{1}H NMR (500 MHz, DMSO-d6) δ 8.15 (d, 2H), 7.58 (d, 2H), 7.42 (dd, 2H), 4.30 (t, 4H), 2.59 (t, 4H), 2.07 (m, 4H).

Synthesis of 2,6-DPSAQ

2,6-diiodoanthraquinone was synthesized according to the reported procedure.[47] Heat a mixture of 2 g 2,6-diiodoanthraquinone (4.35 mmol), 0.75 g sodium allylsulfonate (5.22 mmol), 0.72 g potassium carbonate (5.22 mmol) and 49 mg

palladium acetate(0.22 mmol) in 40 mL water in a pressure vessel to 120 °C for overnight. The mixture solution was filtered to remove insoluble gradients. Collect the filtrate and add it to a 20 mL methanol. The solution was stirred in a hydrogen atmosphere for overnight.

Evaporate the solution in vacuum to collect the solid. Yield: 1.51 g (70%).

The ^{1}H NMR spectrum of 2,6-DPSAQ is shown in Figure S4.

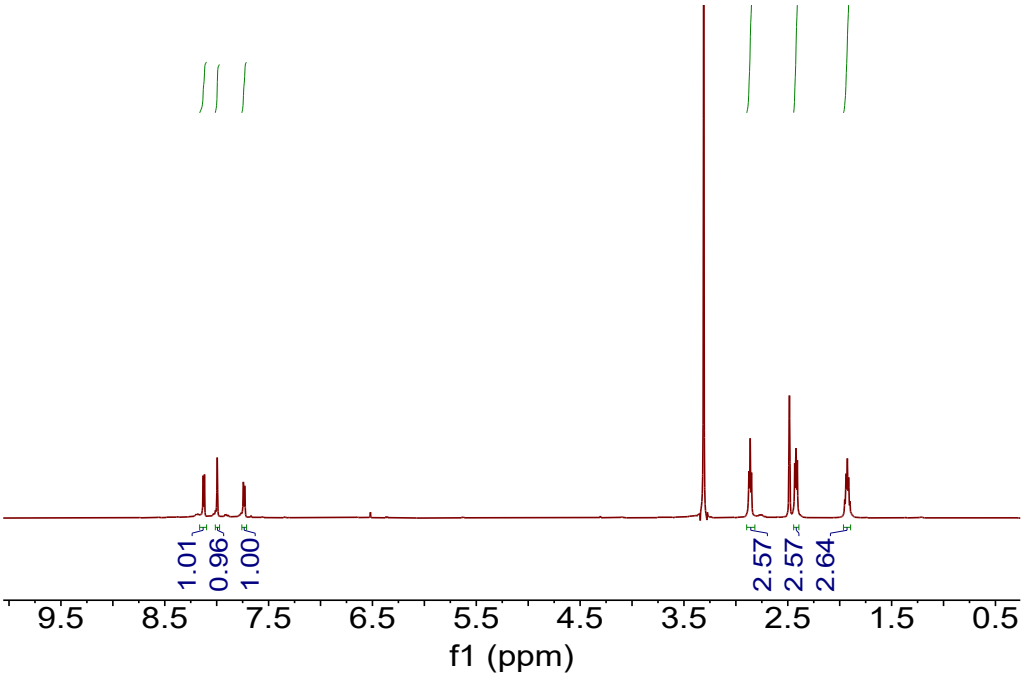

Figure S4. ^{1}H NMR spectrum of 2,6-DPSAQ in DMSO-d6. Solvent peaks are those not integrated. ^{1}H NMR (500 MHz, DMSO-d6) δ 8.12 (d, 2H), 7.99 (d, 2H), 7.74 (dd, 2H), 2.86 (t, 4H), 2.42 (t, 4H), 1.93 (m, 4H).

Table S1. The lab-scale cost of 2,6-DHAQ, 2,6-DAAQ and 1,3-propanesultone are from Sigma-Aldrich in July 2021.

Molecules	Lab-Scale Cost ($/Mol)
2,6-DHAQ	364
2,6-DAAQ	6918
1,3-propanesultone	77

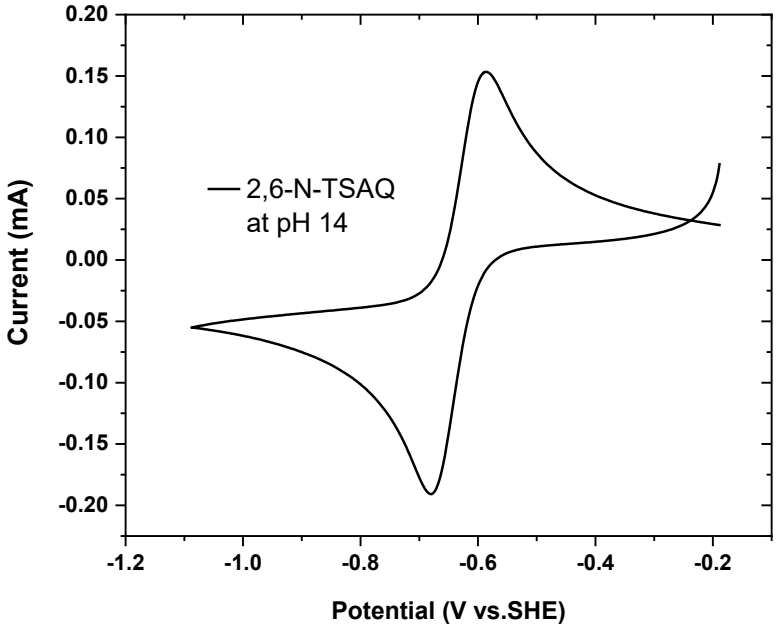

Figure S5. Cyclic voltammograms of 5 mM 2,6-N-TSAQ in 1 M sodium hydroxide at a scan rate of 100 mV/s.

UV-vis and permeability measurements

UV-vis absorbance spectra for calibration curves and crossover detection were taken using an Agilent 8453 spectrophotometer. The permeability of 2,6-N-TSAQ through Nafion NR212 cation

exchange membrane was measured in a custom two-compartment diffusion cell ("H-cell") made by Adams & Chittenden scientific glassware. The Nafion NR212, received protonated, was ion exchanged to sodium form in 1 M NaOH by soaking for over 12 hours at ambient temperature. This membrane was sealed between a donating compartment containing 10 mL of 0.1 M 2,6-N-TSAQ in 1 M NaOH and a receiving compartment containing 10 mL of 0.17 M Na_2SO_4 in 1 M NaOH. The electrolyte in the receiving compartment was designed to minimize osmotic pressure gradients influencing permeability: a freezing point osmometer (Advanced Instruments Inc., Model 3300) confirmed the osmolarity difference between the compartments was only 0.018 Osm. Both compartments were stirred continuously using magnetic stir bars.

Three identical H-cells stirred for 13 days, and 2 mL aliquots were periodically removed from the receiving side to measure absorbance spectra, which were then replaced with fresh receiving solution. Due to the exceptionally low crossover rate, the spectrophotometer was unable to detect the peaks characteristic of 2,6-N-TSAQ, so an upper limit was assigned based on the highest absorbance value observed at 455 nm during the experiment (Fig S8). Using the derivation of Fick's Law reported previously,[1] 2,6-N-TSAQ cannot exceed 3×10^{-14} cm^2/s under these conditions.

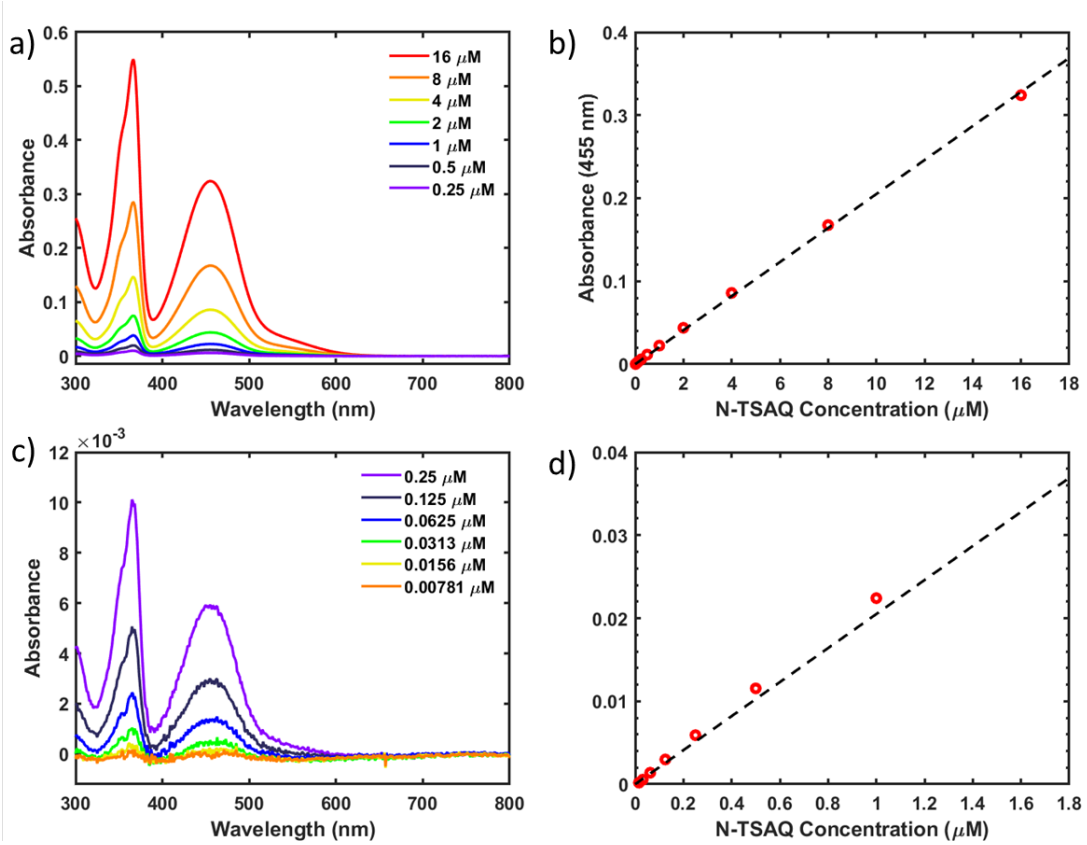

Figure S6. UV-vis absorbance spectra for 2,6-N-TSAQ at concentrations of a) 16 µM to 0.25 µM and c) 0.25 µM to 0.00781 µM in 1 M NaOH. Solutions were prepared by serial 2:1 dilution approaching the detection limit of the spectrophotometer. A baseline of zero absorbance at 750 nm was applied to all spectra. The slope of the resulting calibration curve in panels b) and d) (10x zoom in to the origin of b) gives a molar attenuation coefficient of 0.0205 $\mu M^{-1}cm^{-1}$.

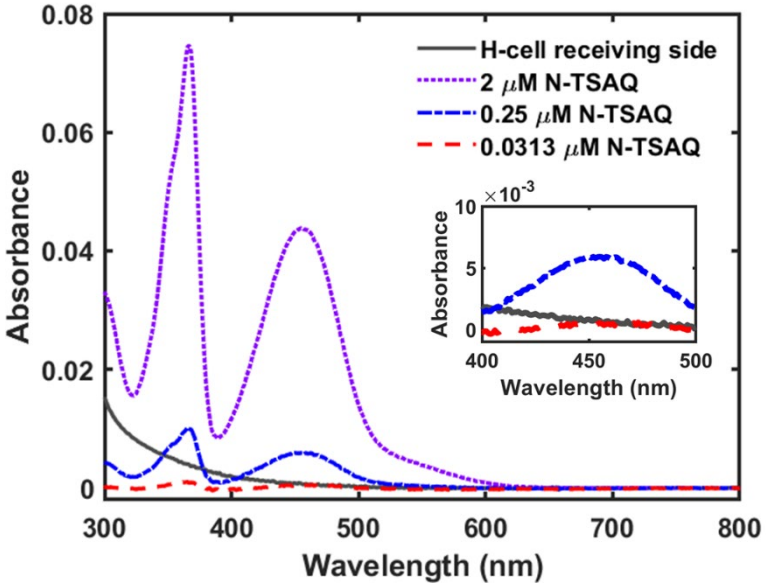

Figure S7. UV-vis of H-cell measurement. The grey trace is the UV-vis absorbance spectrum of the receiving solution of a two-compartment diffusion H-cell which exhibited the highest absorbance at 455 nm over 13 days. This absorbance was used to calculate an upper limit on the permeability of 2,6-N-TSAQ through Nafion NR212 because the peaks indicative of 2,6-N-TSAQ were not detectable by the spectrophotometer. Therefore, the permeability cannot be greater than 3×10^{-14} cm^2/s. The small absorbance at 300-400 nm indicates a minor impurity which does not interfere with the 2,6-N-TSAQ peak at 455 nm.

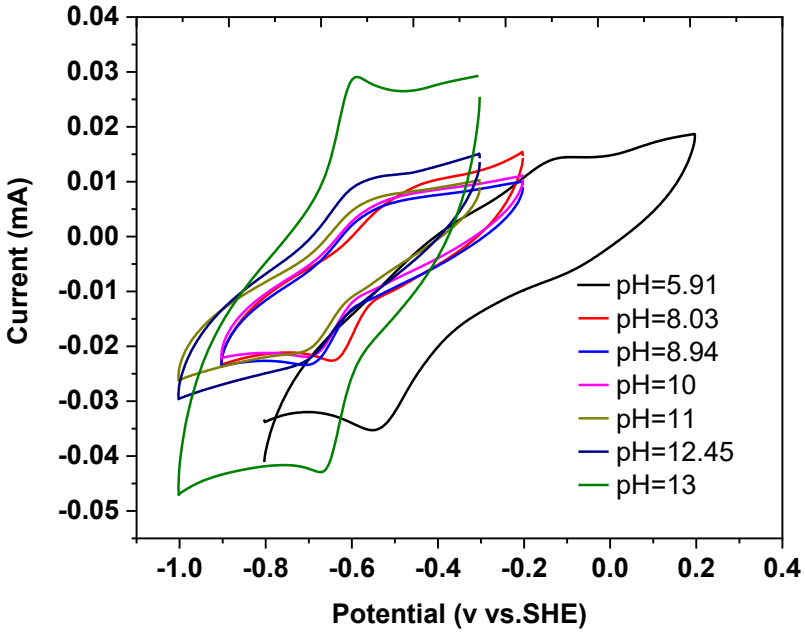

Figure S8. CV of 2 mM 2,6-N-TSAQ in different pH buffer solutions at a sweep rate of 100 mV/s.

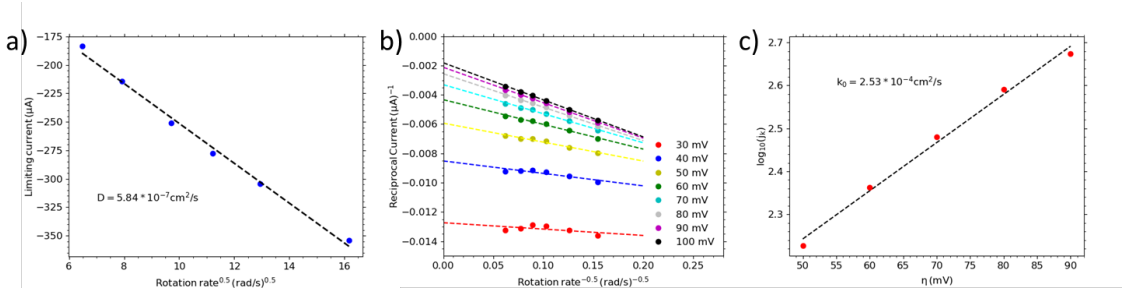

Figure S9. Electrochemical kinetics of 2,6-N-TSAQ in 1 M NaOH. a) Levich plot (limiting current versus square root of rotation rate) of 5 mM 2,6-N-TSAQ in 1 M NaOH. Limiting current is taken as the current at -0.8 V vs SHE in Figure 3b. The slope yields a diffusion coefficient for the 2,6-N-TSAQ of 5.84×10^{-7} cm^2/s; b) Koutecký-Levich plot (reciprocal current versus inverse square root of rotation rate) of 5 mM 2,6-N-TSAQ in 1 M NaOH; c) Fitted Tafel plot of 5 mM 2,6-N-TSAQ in 1 M NaOH. The charge transfer coefficient is calculated to be 0.32, and the rate constant is calculated to be 2.53×10^{-4} cm/s.

Full cell measurements

Flow battery experiments were performed with cell and hardware from Fuel Cell Tech. (Albuquerque, NM). Pyrosealed POCO graphite flow plates with serpentine flow designs were used for both electrodes. Each electrode comprised a 5 cm^2 geometric surface area enclosed by one piece of AvCarb carbon electrode. For 2,6-N-TSAQ/ferrocyanide full cell tests, a Nafion^{TM} 212 membrane was used to serve as the ion-selective membrane. The Nafion membrane was soaked in the supporting electrolyte (sodium hydroxide or sodium chloride) for at least 24 hours before use. Viton sheets were used to cover the outer portion space between the electrodes. Torque used for cell assembly was 60 lb-in (6.78 Nm) on each of eight 1/4-28 bolts. The electrolytes were input into the cell through fluorinated ethylene propylene (FEP) tubing at a rate of 60 mL/min, controlled by Cole-Parmer 6 Masterflex L/S peristaltic pumps. The cell was run inside a glove box (1 ppm O_2). Cell polarization measurements and charge-discharge cycling were conducted using a Biologic BCS-815 battery cycler. Long-term cycling of the 0.1 M 2,6-N-TSAQ/ferrocyanide cell was achieved at ±40 mA cm^{-2} with potential holds at 1.4 V for charging and 0.6 V for discharging until the current density dropped to 2 mA cm^{-2}. The polarization curves were obtained by charging to a desired state of charge first and then polarizing via linear sweep voltammetry at a rate of 100 mV s^{-1}.

A glassy carbon (BASi, 3 mm diameter) working electrode, an Ag/AgCl reference electrode (BASi, 3 M NaCl solution), and a graphite counter electrode were used in the three-electrode system for all CV tests.

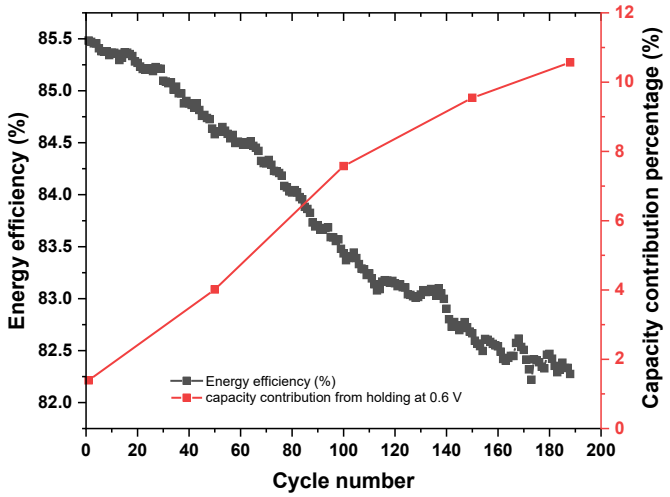

Figure S10. Energy efficiency and capacity contribution percentage at voltage hold at 0.6 V versus cycle number of the 0.1 M 2,6-N-TSAQ/ferrocyanide cell in 1 M sodium chloride solution.

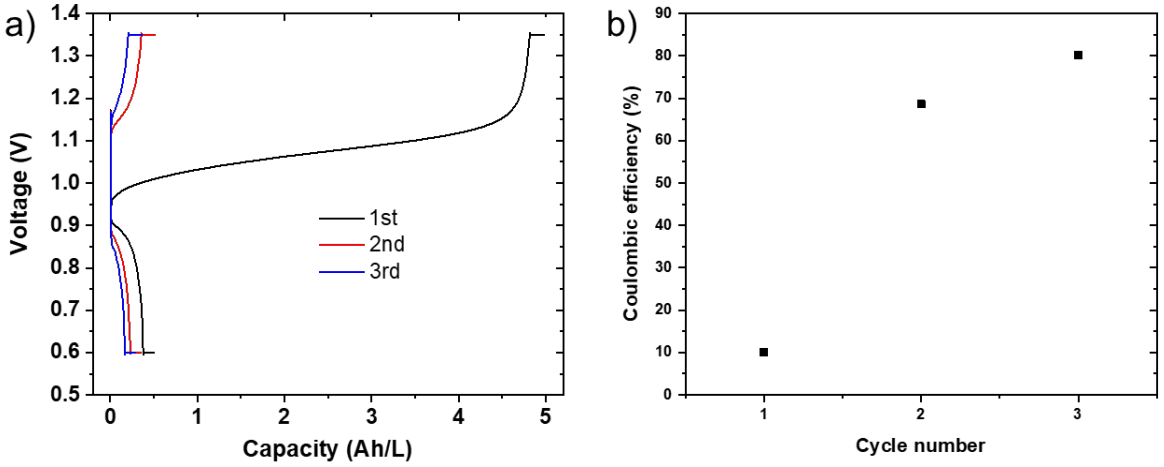

Figure S11. Cell performance of 0.1 M 2,6-N-TSAQ/ferrocyanide cell in 1M NH_4Cl supporting electrolyte. a) Charge-discharge voltage profile of 0.1 M 2,6-N-TSAQ/ferrocyanide full cell in 1 M NH_4Cl at pH 7. b) The corresponding coulombic efficiency for 0.1 M 2,6-N-TSAQ/ferrocyanide cell in 1 M NH_4Cl condition. Cell condition: 5 mL 0.1 M 2,6-N-TSAQ in 1 M NH_4Cl as the negolyte, and 30 mL 0.1 M $K_4Fe(CN)_6$ and 0.02 M $K_3Fe(CN)_6$ in 1 M NH_4Cl as the posolyte, both electrolytes are tuned to pH 7 with sodium hydroxide.

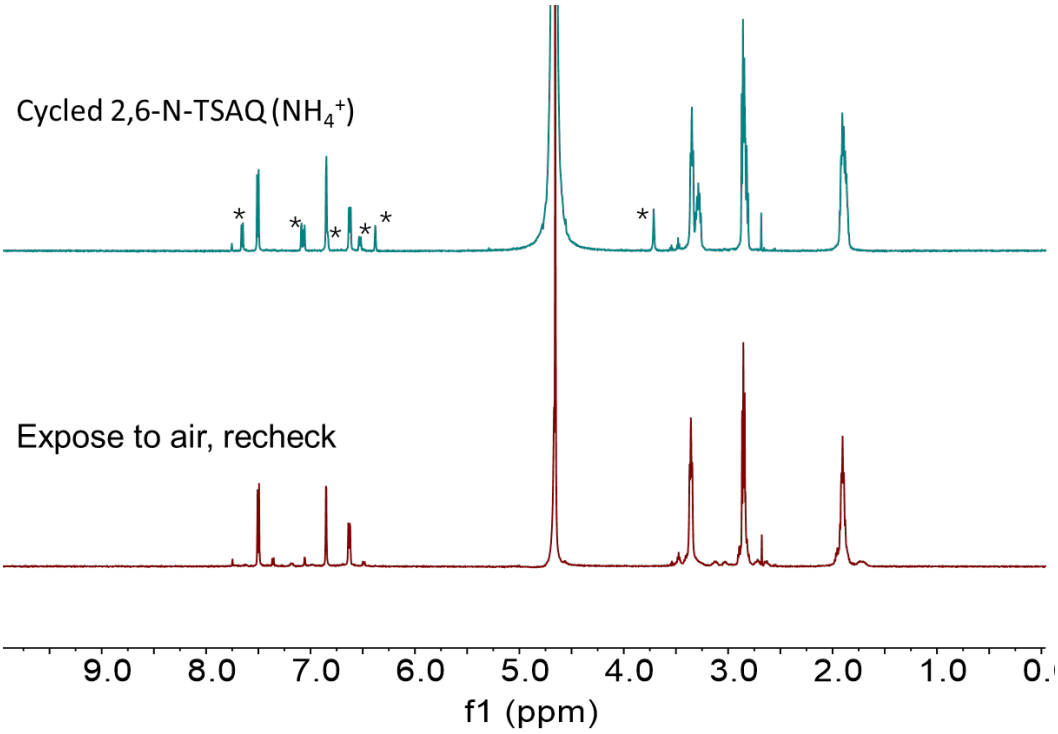

Figure S12. ^{1}H NMR spectra (500 MHz) of the cycled 2,6-N-TSAQ in 1 M NH_4Cl electrolyte diluted with 5 volumes of D_2O solvent. The asterisk peaks belong to anthrone, after fully air aerated, the anthrone peaks disappeared.

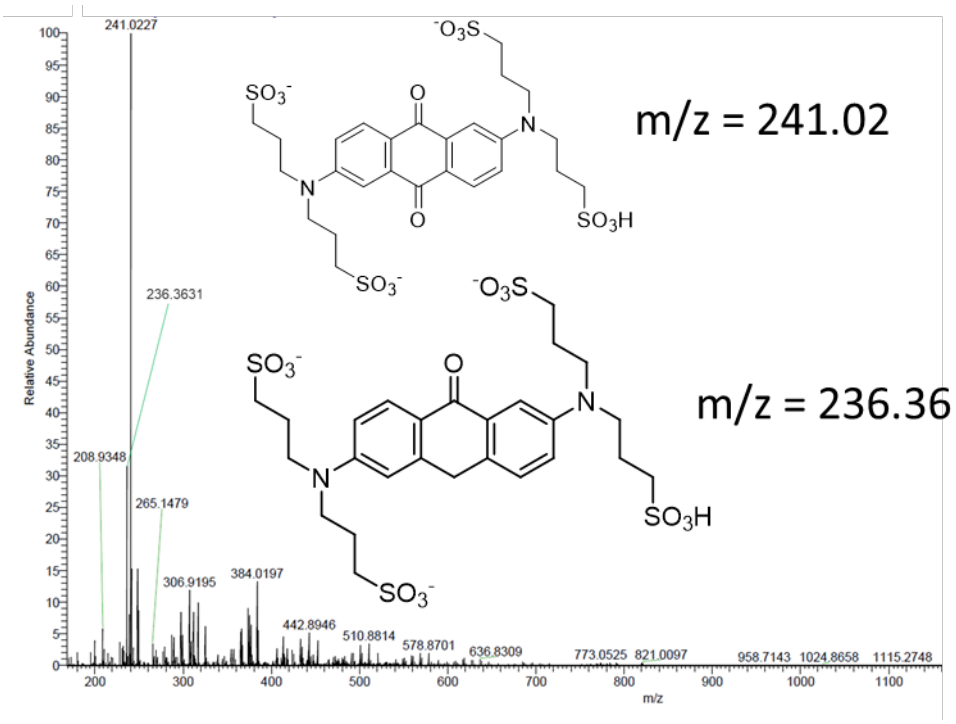

Figure S13. The mass spectrum of the cycled 2,6-NTSAQ (NH_4Cl) electrolyte. The electrolyte was diluted 10,000 times with HPLC water and directly analyzed with mass spectrometry. The m/z peak at 236.36 belongs to the anthrone peak, and peak at 241.02 belong to 2,6-N-TSAQ.

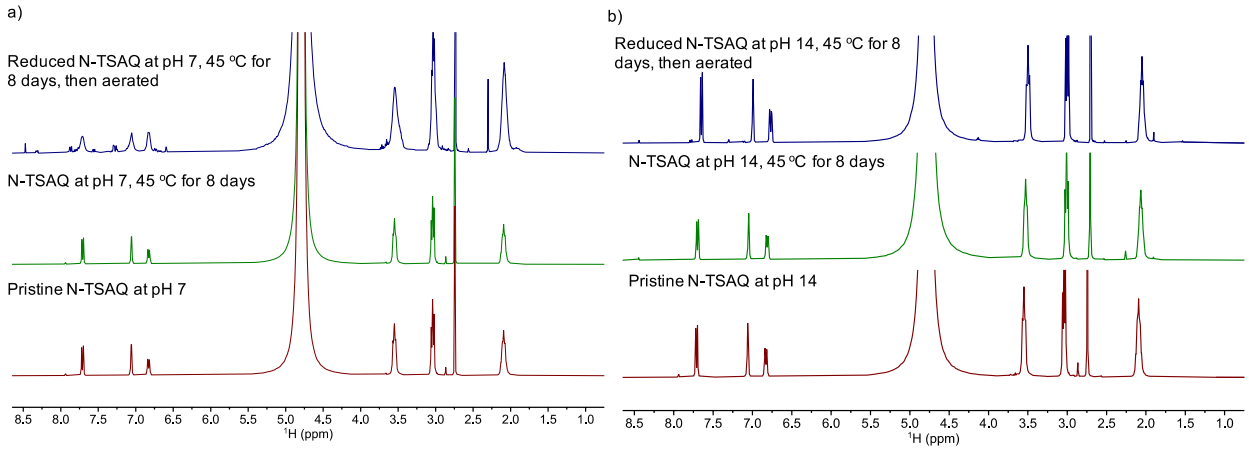

Figure S14. ^{1}H NMR spectra (400 MHz) of 2,6-N-TSAQ in D_2O solvent. (a) from bottom to top: pristine 2,6-N-TSAQ; 0.1 M 2,6-N-TSAQ in 1 M NaCl at 45 °C for 8 days; 0.1 M reduced form of 2,6-N-TSAQ in 1 M NaCl at 45 °C for 8 days, then aerated; (b) from bottom to top: pristine 2,6-N-TSAQ; 0.1 M 2,6-N-TSAQ in 1 M NaOH at 45 °C for 8 days; 0.1 M reduced form of 2,6-N-TSAQ in 1 M NaOH at 45 °C for 8 days, then aerated.

References

1. Kwabi, D. G.; Lin, K.; Ji, Y.; Kerr, E. F.; Goulet, M.-A.; De Porcellinis, D.; Tabor, D. P.; Pollack, D. A.; Aspuru-Guzik, A.; Gordon, R. G.; Aziz, M. J., Alkaline quinone flow battery with long lifetime at pH 12. *Joule* **2018,** *2* (9), 1907-1908.